ACS OMEGA

http://pubs.acs.org/journal/acsodf
Article

Theoretical Insights into the Structural and Optical Properties of D−π−A-based Cyanostilbene Systems of α and β Variants

Cherumannil Femina, Pookkottu K. Sajith,* Karunakaran Remya, Reji Thomas, and Rajadurai Vijay Solomon*

Cite This: *ACS Omega* 2024, 9, 22764−22776
Read Online

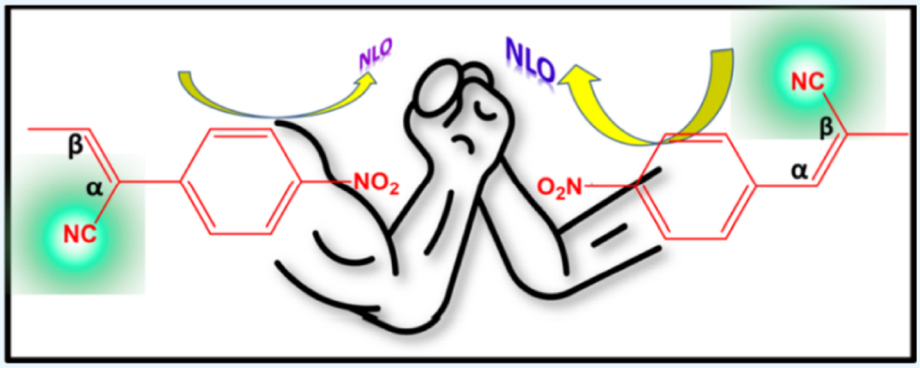

ABSTRACT: The π-conjugated organic molecules containing cyanostilbene motifs have been extensively investigated due to their great potential applications in several optoelectronic and biological fields. Developing efficient molecules in this respect requires strategic structural engineering and a deep understanding of the structure−property relationship at the molecular level. In this context, understanding the impact of positional isomerism in cyanostilbene systems is a fundamental aspect of designing desired materials with improved photophysical properties. Herein, we designed ten donor−π−acceptor (D−π−A) type cyanostilbene derivatives ($\mathbf{P_1} - \mathbf{P_{10}}$) with different π linkers and compared their structural and optoelectronic properties arising from the positional variations of the −CN group (α and β- variations) through the utilization of density functional theory (DFT) and time-dependent DFT (TDDFT) methods. The topological analyses of the electron density are used to explain the relatively high stability of α isomer compared to that of β. Frontier molecular orbital analysis reveals that 17 molecules tend to show a reduced highest occupied molecular orbital−lowest unoccupied molecular orbital gap, and most of them showed a greater nonlinear optical (NLO) character compared to the parent molecule. TDDFT calculations indicate that β isomers show higher absorption maxima compared to their α counterparts. Among all the scrutinized molecules, the absorption maximum extended up to 602 nm for $\mathbf{P_9}$ and it possesses the highest first-order hyperpolarizability. This study sheds light on positional isomers and their reactivity, absorption spectra, and NLO properties of D−π−A type architecture that can be suitably tuned by appropriating the π-bridge for practical applications.

1. INTRODUCTION

Stimuli-responsive materials with different π-conjugated structures have evolved as new-generation functional materials due to their intriguing optoelectronic properties and their subtle tunability.[1,2] Among the π-conjugated molecular systems, cyanostilbene-based assemblies are the most promising candidates for various optoelectronic applications owing to their aggregation-induced enhanced emission properties (AIEE).[3−5] Literature shows that the cyanostilbene derivatives are employed as multifunctional building blocks for various applications such as organic solar cells, organic field effect transistors, organic light-emitting diodes, liquid crystal displays, bioimaging, sensing, etc.[4,6−11] In addition, the cyanostilbene systems are well explored for the response to multiple stimuli such as pressure, temperature, light, solvent, and pH.[5,12−14]

The functional motif in cyanostilbene consists of π-conjugated skeletons, which are covalently linked to a cyano group. The insertion of the cyano substituent at different positions in the core stilbene unit is one of the most powerful means of fine-tuning the physicochemical properties of cyanostilbene.[15] The positional isomers thus obtained in which the −CN group that is connected at the α-position of the ethylenic bond is called α-cyanostilbene, whereas the −CN

Received: January 25, 2024
Revised: April 21, 2024
Accepted: April 23, 2024
Published: May 15, 2024

https://doi.org/10.1021/acsomega.4c00850
ACS Omega 2024, 9, 22764−22776

group connected at the β-position is termed as β-cyanostilbene.[3] Generally, these two positional isomers of acrylonitrile have variable molecular arrangements that influence the crystal packing characteristics.[16] For instance, a report by Zhang et al. demonstrated that the molecular packing and optical properties are greatly affected by the positions of the cyano group on donor−acceptor type isomers.[17] Yoon et al. explored the tunability of photophysical features of a series of α and β cyanostilbene derivatives and the report implied the advantages of position and orientation of the cyano unit in controlling the solution and solid state photophysical properties.[4] An investigation by Ros and co-workers on cyanostilbene-based bent-core liquid crystals demonstrated the control of positional isomerism on the molecular arrangement and fluorescence properties in the liquid crystalline states.[9] The study established that the quantum yields depend on the position of the cyano group and the value is higher for the β-isomer than that of the α-isomer due to the higher radiative and lower nonradiative rates of the β-isomer. A report on two distyrylpyrrole derivatives with α and β cyano substitution resulted in substantial differences in solid-state luminescence behavior.[18] From all of these experimental reports, it is evident that the position of the cyano group plays a significant role in deciding and dictating the extent of conjugation, molecular packing, and photophysical properties of a molecule. However, there are very few experimental reports that link positional isomerism in cyanostilbenes evolved by the position of the cyano group to the observed difference in optical properties in the solution and solid states, so far.[16,19−21] Furthermore, to the best of our knowledge, the structural, energetics, and optical properties of α and β analogs of cyanostilbene have not been systematically compared and explored. In this scenario, a molecular-level understanding through theoretical approaches will guide us in gaining insights into such properties and offer valuable guidelines for designing efficient optoelectronic candidates for practical applications.

Cyanostilbene appended donor−π−acceptor (D−π−A) type systems, where the cyano moiety acts as the acceptor (A), are the more straightforward model for a comprehensive understanding of the effect of positional isomerism of α and β analogs of cyanostilbene because it allows flexibility in molecular design by changing either conjugating moiety (π) or donor unit (D) systematically.[6,22−24] Such systems are capable of fabricating excellent hole and electron transport facilities and executing push−pull effects, allowing electron transfer from the donor to the acceptor through the conjugated π-units.[25−29] Furthermore, D−π−A architecture having functionalized acrylonitrile compounds offers better nonlinear optical (NLO) performance.[30−32] For example, Singh and co-workers recently synthesized a series of cyanostilbene-based D−π−A systems containing the 9,9-dimethyl-9*H*-fluoren-2-amine type of chromophores and observed a significant enhancement in the first hyperpolarizability and related intrinsic hyperpolarizability by modulating the π-conjugation pathways.[30] In a continued work,[31] the same group compared the first hyperpolarizabilities by extending the π-conjugation of D−π−A systems and found that lengthening of π-conjugation beyond a certain limit hardly improves the NLO response. Therefore, improving the efficiency through structural tuning to design better NLO candidates attracts a lot of attention.[33−36] In recent years, organic heterocyclic luminophores have made great progress as a new-generation functional material.[37−39] These findings triggered our curiosity to computationally design cyanostilbene-based NLO materials with various heterocyclic rings as π-linkers.[29,40] More importantly, it would also serve as the optimal candidate to study the effect of positional isomerism on the cyanostilbene derivatives.

Motivated by the above-mentioned considerations, herein we employed a systematic comparative study focusing on the structural properties, orbital analysis, and relative stabilities of α and β analogs (respectively designated as "**a**" and "**b**" isomeric forms, hereafter) of various cyanostilbene derivatives with the help of density functional theory (DFT) calculations. The cyanostyryl appended D−π−A systems with varying π linkers have been designed for this purpose. The absorption characteristics of these compounds are judiciously investigated using time-dependent DFT (TDDFT) studies. The present study additionally examines the impact of various π linkers on the NLO properties of the designed molecules. Bader's quantum theory of atoms in molecules (QTAIM),[41,42] noncovalent interaction (NCI),[43] and molecular electrostatic potential (MESP)[44] analyses have been performed to further understand the structure−property evaluation of these molecules.

2. THEORETICAL CALCULATIONS

All DFT and TDDFT calculations are performed using the Gaussian 16 suite of programs.[45] The geometry optimizations followed by frequency calculations of all molecules are done in the gaseous state at the B3LYP/6-31+G(d,p) level of theory.[46,47] Vibrational frequency calculations confirm that all of the reported geometries correspond to true minima, ensuring the absence of imaginary frequencies.

The Frontier molecular orbital (FMO) analysis is done with the optimized geometries of the designed molecules and FMOs are plotted using the Chemcraft software.[48] QMForge program[49] is used for the FMO percentage analysis to understand the role of the donor, acceptor, and the π-bridge toward the stabilization of highest occupied molecular orbital (HOMO) and lowest unoccupied molecular orbital (LUMO) of these molecules.

From the optimized geometries, topological analyses of the designed molecules are performed using the B3LYP/6-31+G(d,p) method. The wfn files generated from the Gaussian outputs are used for this purpose. NCI[43] and QTAIM[42] analyses are computed using the Multiwfn[50] and AIMAll[51] software, respectively. The reduced gradient density (RDG) isosurface plots resulting from NCI analysis are further visualized using the VMD package.[52]

The literature shows plenty of functionals capable of predicting the absorption maxima and, therefore, it is highly essential to identify and validate the correct functional that can reproduce the experimental results in cyanostilbene systems. In this context, to identify the suitable functional to simulate the experimental absorption maxima in the solution state of these cyanostilbene derivatives, all computations including geometry optimizations and subsequent time-dependent DFT (TD-DFT) calculations were performed with different functionals *viz.* B3LYP, CAM-B3LYP,[53] PBE0,[54] and Boese−Martin for Kinetics (BMK)[55] coupled with the 6-31+G(d,p) basis set. The Solvation Model based on Density (SMD) solvation model[56] with the relevant solvent reported in the experimental work was adopted for these calculations. Figure S1 shows the selected molecules ($\mathbf{P_0a}$,[30] **1**,[10] **2**,[11] and **3**[14]) for the simulation of absorption spectra. The graphical comparison of the

https://doi.org/10.1021/acsomega.4c00850
ACS Omega 2024, 9, 22764−22776

absorption maxima (λ_{max}) obtained using different functionals calculated at the TD/DFT/SMD/6-31+G(d,p) level is displayed in Figure 1. It is clear from Figure 1 that the BMK

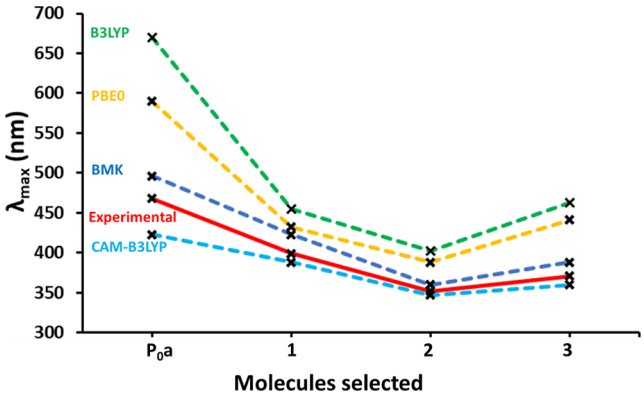

Figure 1. Graphical comparison of the experimentally reported absorption maxima of selected molecules to the corresponding simulated values. Solid curve corresponds to the experimentally reported values, and broken curves represent simulated values obtained using different functionals.

is the best functional for the simulation of absorption spectra since it gives λ_{max} values that are consistently in agreement with the experimental values. Indeed, the CAM-B3LYP results are closer to the experimental results of the three systems, but **P_0a** shows a significant deviation. This suggests that the BMK method is better suited to TDDFT calculations for the present study. In addition, there have been some previous reports suggesting the use of the BMK method for the study of absorption spectra in organic compounds.[57,58] In fact, Table S1 (Supporting Information) shows that the λ_{max} calculated at the TD-BMK/SMD/6-31+G(d,p) level from the gas phase optimized geometries of B3LYP/6-31+G(d,p) agrees well with the experimentally observed λ_{max}. Subsequently, this methodology was adopted herein for the computation of the vertical excitations and oscillator frequency. The simulated absorption spectral data are analyzed using the GaussSum software.[59]

The optimized geometries at the B3LYP/6-31+G(d,p) level were used to compute first- and second-order hyperpolarizabilities to characterize the NLO activity of the designed molecules. The first-order hyperpolarizability (β_0), described by a 3 × 3 × 3 matrix, is computed from the x, y, and z hyperpolarizability tensor components using the eq 1.[60]

$$\beta_0 = [(\beta_{xxx} + \beta_{xyy} + \beta_{xzz})^2 + (\beta_{yyy} + \beta_{yzz} + \beta_{yxx})^2 + (\beta_{zzz} + \beta_{zxx} + \beta_{zyy})^2]^{1/2} \quad (1)$$

Second-order hyperpolarizability (γ) is calculated from its components using the eq 2.[60]

$$\gamma = 1/5[\gamma_{xxxx} + \gamma_{yyyy} + \gamma_{zzzz} + 2(\gamma_{xxyy} + \gamma_{yyzz} + \gamma_{xxzz})] \quad (2)$$

3. RESULTS AND DISCUSSION

Twenty different D−π−A systems derived from an experimentally reported structure **P_0a** (Figure 2A)[30,31] are designed and considered for the present study. All the designed molecules are cyanostyryl-based structures with a dimethylamino group as the donor and a cyano-substituted nitrostyryl

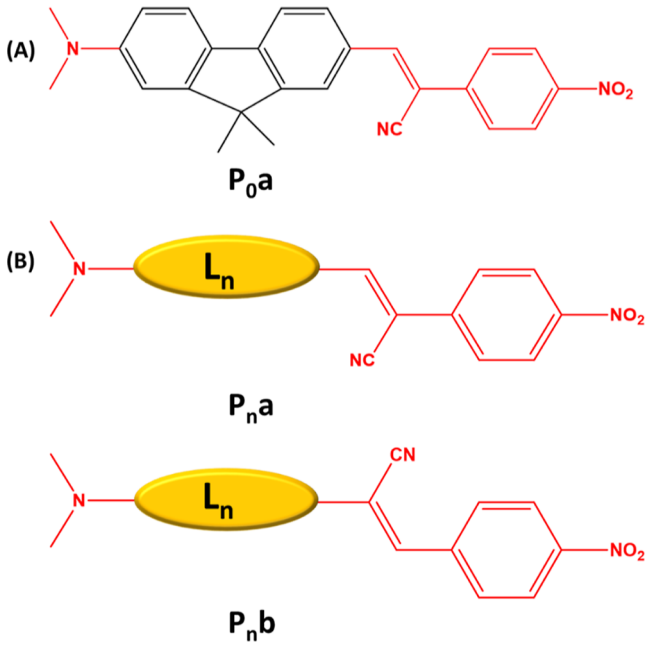

Figure 2. (A) Reference system considered and (B) the isomers ("**a**" and "**b**" variants) investigated in this study.

group as the acceptor part. The cyano group here functions as an additional electron-withdrawing group in the D−π−A structure. The initial geometry of the reference molecule **P_0a** is taken from the X-ray crystallographic data.[30] Molecules with ten different spacer groups (π bridges, designated as **L_n**), each having "**a**" and "**b**" forms with respect to the position of the −CN group, as shown in Figure 2B, have been included in the study. Hence, a total of 20 D−π−A architectures have been examined to understand the role of π-linkers as well as the positioning effect of the −CN group on their structural and optoelectronic properties. In addition, the reference compound **P_0a** and its positional isomer **P_0b** are also considered for comparison. The different spacer groups used in designing the D−π−A systems are shown in Figure 3. The selected spacer groups include aromatic π-conjugated systems of phenyl-based and heterocyclic rings containing heteroatoms such as nitrogen, oxygen, and sulfur (see Figure 3).[61,62]

3.1. Optimized Molecular Geometries. Optimized geometries of four representative molecules *viz.* **P_1a**, **P_1b** (with no heteroatom in the spacer group), **P_3a**, and **P_3b** (with oxygen as the heteroatom in the spacer group) are shown in Figure 4. As can be seen in the figure, **P_na** and **P_nb** possess the same D−π−A backbone with only a difference in the position of the −CN group. The computed dihedral angles Φ_1 and Φ_2, as indicated in Figure 4, have been considered for analyzing the planarity of the systems under study. Φ_1 is the $C\alpha C_\beta C_1 C_2$ dihedral angle (where C_α and C_β are the α and β carbon atoms and to which the −CN group is attached in the "**a**" and "**b**" isomers, respectively, and C_1 and C_2 are two carbon atoms of the phenyl ring of the styryl group) and Φ_2 is a C−C−C−C/X (where "X" is the heteroatom) dihedral angle inside the spacer group, as illustrated in Figure 4. The dihedral angle Φ_2 is not significant for the two **P_0** molecules because spacer group **L_0** does not contain a phenyl ring that is connected to the remaining part of the π-spacer through a single bond. The Φ_1 and Φ_2 values of all of the D−π−A systems under study are listed in Table S2. All the scrutinized molecules are distorted

https://doi.org/10.1021/acsomega.4c00850
ACS Omega 2024, 9, 22764−22776

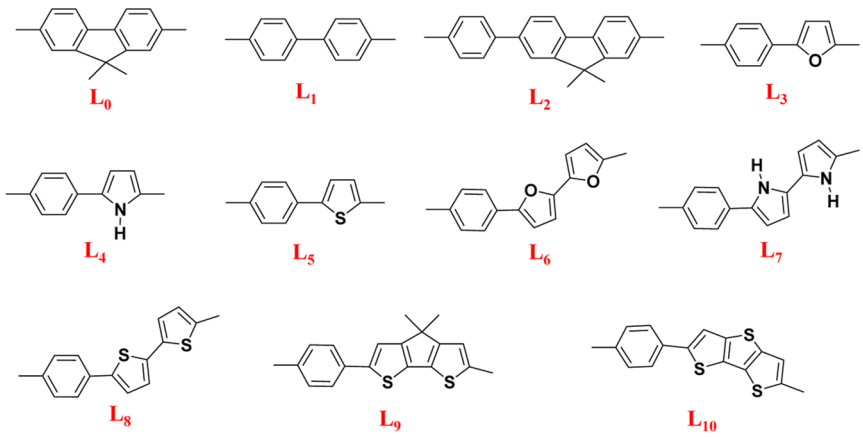

Figure 3. Sketches of the π-spacers used in the study.

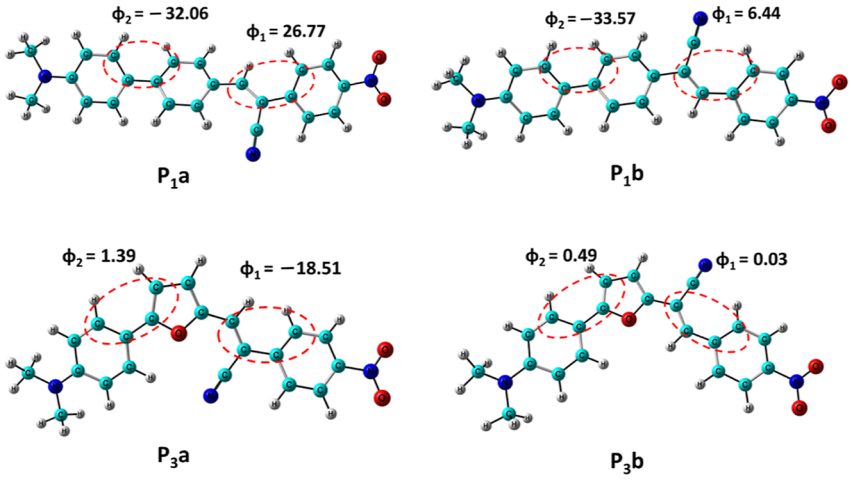

Figure 4. Optimized geometries of the representative structures. The two dihedral angles Φ_1 and Φ_2 (in degrees) are also shown.

from planarity to different extents. As can be observed from Table S2, there is a significant decrease in the value of Φ_1 (~10 to 20°) in the "**b**" series, as compared to the "**a**" series, indicating a remarkable increase in planarity as the position of the −CN group changes from "**a**" to "**b**" positions. The lower values Φ_1 indicate less distortion of "**b**" forms and a slightly higher conjugation effect. Molecules such as $\mathbf{P_{10}b}$, $\mathbf{P_9b}$, $\mathbf{P_8b}$, and $\mathbf{P_5b}$ having sulfur-containing heterocyclic rings possess very small Φ_1 values (less than 1°) leading to more efficient π-delocalization in the backbone. The smaller values of dihedral angles for molecules with heteroatoms in their spacer groups indicate higher planarity in them compared to those without heteroatoms. As indicated by the small dihedral angles, $\mathbf{P_3b}$ and $\mathbf{P_6b}$, both having furanoid rings in their spacer groups, possess the highest planarity. Among all of the systems studied, $\mathbf{P_6}$ possesses the lowest Φ_2. In all the designed molecules, the delocalization of π-electrons throughout the molecule is evident from the calculated geometrical parameters and dihedral angles.

Analyzing the different bond lengths in the positional isomers has shown that in all the cases, the "**b**" isomer has a slightly shorter −C−N bond (Table S2). The increased planarity as indicated by the dihedral angle and better π delocalization slightly increased the −C−N bond strengths in the "**b**" isomers.

The calculated dipole moments of all designed molecules are also presented in Table S2. From Table S2, it is clear that most of the molecules showed a higher dipole moment compared to that of reference molecule $\mathbf{P_0a}$ (12.51 D). Among all of the scrutinized molecules, the highest dipole moment of 16.07 D is exhibited by $\mathbf{P_9a}$. The dipole moments of the isomers "**a**" and "**b**" are quite similar, indicating that the net molecular polarity is not much affected by positional changes.

3.2. Relative Stabilities of "a" and "b" Forms. Next, we examined the energies of the isomeric structures "**a**" and "**b**" to assess their relative stability. The difference in energy between the isomers "**b**" and "**a**" (denoted as ΔE_{ba}; given in Table S2) is noted. In all cases, ΔE_{ba} is positive, indicating that the isomer "**a**" is more stable than "**b**". This may be attributed to the possibility of additional intramolecular interactions in the "**a**" isomer, which needs to be further confirmed by analyzing the electron density topology analyses. ΔE_{ba} values in all cases are compared with the help of bar diagrams provided in Figure 5. It is obvious that $\mathbf{P_4a}$ and $\mathbf{P_7a}$ exhibit more stability (ΔE_{ba} values of 7.4 and 7.1 kcal/mol, respectively) than the corresponding "**b**" analog. The lowest ΔE_{ba} value of 1.2 kcal/mol is noted for $\mathbf{P_1}$ isomers.

3.3. NCI and QTAIM Analyses. NCI and QTAIM analyses serve as a valuable tool to identify, visualize, and quantify various inter and intramolecular chemical interactions present in molecular systems.[63−65] We further performed NCI and QTAIM analyses to unravel various NCIs present within the designed molecules. As shown in Figure 6, the RDG isosurfaces resulting from the NCI analysis of representative

https://doi.org/10.1021/acsomega.4c00850
ACS Omega 2024, 9, 22764−22776

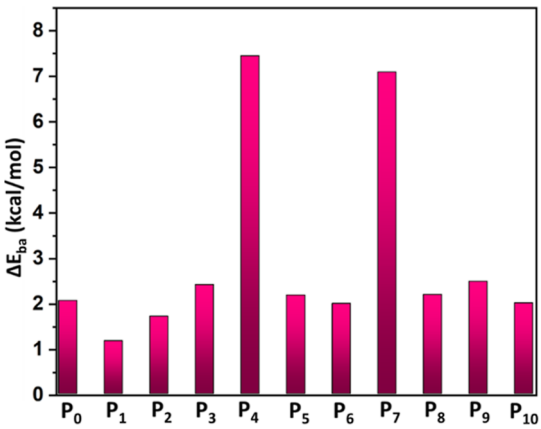

Figure 5. Bar chart representation of the calculated ΔE_{ba} values of the studied molecules.

isomeric pairs $\mathbf{P_4}$ and $\mathbf{P_7}$ are shown. The color scheme and the area of the isosurface serve as a convenient means of understanding the nature of NCIs.[43] For instance, the red zones correspond to repulsive interactions, whereas the green zones are indicative of weak van der Waals interactions. In Figure 6, the appearance of green zones shows the attractive intramolecular interactions present in these systems. A close examination of the NCI isosurface indicates that the "**a**" isomers have a slightly larger area of green isosurfaces compared to their "**b**" counterparts, particularly around the −CN centers. This shows that the attractive intramolecular interactions present in the "**a**" isomer are greater compared to the "**b**" isomer.

On the other hand, the QTAIM analysis uncovers not only the occurrence of intramolecular NCIs but also the nature of such interactions through the appearance of (3, −1) bond critical points (BCPs).[66,67] These BCPs are characterized by their corresponding electron density (ρ) values. As representative systems, the QTAIM features of two pairs of isomers *viz.* $\mathbf{P_4}$ ("**a**" and "**b**") and $\mathbf{P_7}$ ("**a**" and "**b**") are displayed in Figure 7. $\mathbf{P_4a}$ isomer possesses intramolecular interaction between the H (from the N−H group in the spacer group) and the −C−N group with a ρ at the BCP of 0.01482 au. The −CH(phenyl)···CN interaction (ρ = 0.01282 au) is evident in the QTAIM molecular graph of $\mathbf{P_4b}$. For "**a**", ρ value is larger than that of the "**b**" isomers indicating the stronger interaction present in "**a**". In addition, the existence of another BCP corresponding to CH···HC contact is evident in the "**a**" isomer for both $\mathbf{P_4}$ and $\mathbf{P_7}$. Thus, in line with the NCI plots, the QTAIM analysis clearly suggests that stronger intermolecular interactions are present in "**a**" compared to their "**b**" counterparts; this corroborates the higher ΔE_{ba} values obtained for $\mathbf{P_4}$ and $\mathbf{P_7}$ and thus explains the relatively higher stabilities of "**a**" isomers.

The increased intramolecular interactions of −C−N present in the "**a**" isomer decrease the −C−N bond strength, and consequently the value of ρ at the BCP of −C−N of "**a**" [$\rho_{CN}(\mathbf{a})$] is found to be smaller than their "**b**" counterparts [$\rho_{CN}(\mathbf{b})$], in all cases. $\rho_{CN}(\mathbf{a})$ and $\rho_{CN}(\mathbf{b})$ values of $\mathbf{P_4}$ and $\mathbf{P_7}$ given in Figure 7 in green color. The difference in ρ values at the BCP of −C−N between "**b**" and "**a**" [$\Delta\rho = \rho_{CN}(\mathbf{b}) - \rho_{CN}(\mathbf{a})$] roughly correlates with the ΔE_{ba} values (see Supporting Information; Figure S2 and Table S3). This further confirms that the relatively high stability of the "**a**" isomer originates from intramolecular interactions.

3.4. Molecular Electrostatic Potential Surfaces. The MESP maps provide valuable information about the region around a molecule where an electrophilic and nucleophilic attack is possible.[68] It also gives an idea about the possible NCI of molecules with their surroundings.[69,70] The MESP isosurfaces of the two isomers of the representative systems ($\mathbf{P_4}$ and $\mathbf{P_7}$) are shown in Figure 8. The highest negative potential (red region) is located mainly around the oxygen atoms of $-NO_2$ and N of the −CN group. The MESP isosurfaces shown in Figure 8 indicate that the positive electrostatic potential regions (blue regions) are dispersed around the H atoms present in the molecule. The possibility of intramolecular interaction between −CN and the nearby −NH region of pyrrole is evident from the negative and positive charge localization of the corresponding moieties of the "**a**" isomer (Figure 8).

3.5. Frontier Molecular Orbitals. It is well known that the FMO analysis sheds light on the chemical reactivity, which in turn helps to estimate the optoelectronic properties of D−π−A systems.[71,72] Therefore, the FMOs such as the HOMO and LUMO obtained from the optimized geometries are studied. The calculated energies of HOMO and LUMO together with the HOMO−LUMO energy gap (ΔE_{HL}) are collected in Table S4. The "**a**" isomers show a wider ΔE_{HL} compared to their "**b**" counterpart (see Figure 9 for $\mathbf{P_0} - \mathbf{P_3}$, and the remaining in Figure S3). Among the 22 molecules, $\mathbf{P_1a}$

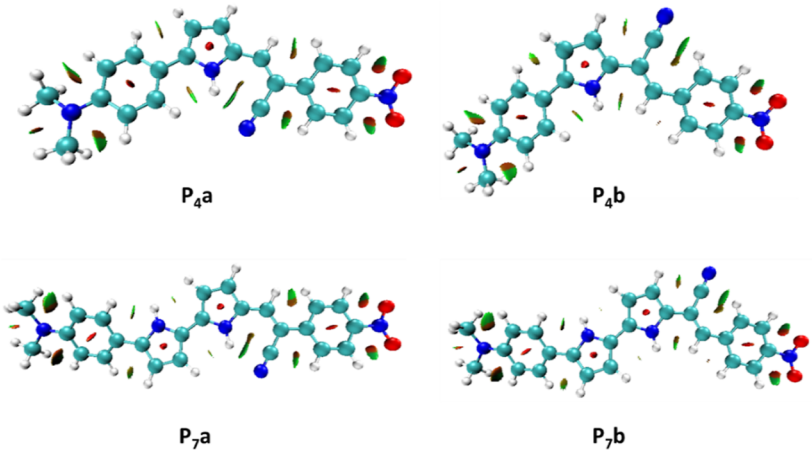

Figure 6. NCI- RDG isodensity surface plot (isovalue = 0.50 au) of $\mathbf{P_4}$ and $\mathbf{P_7}$ isomers.

https://doi.org/10.1021/acsomega.4c00850
ACS Omega 2024, 9, 22764−22776

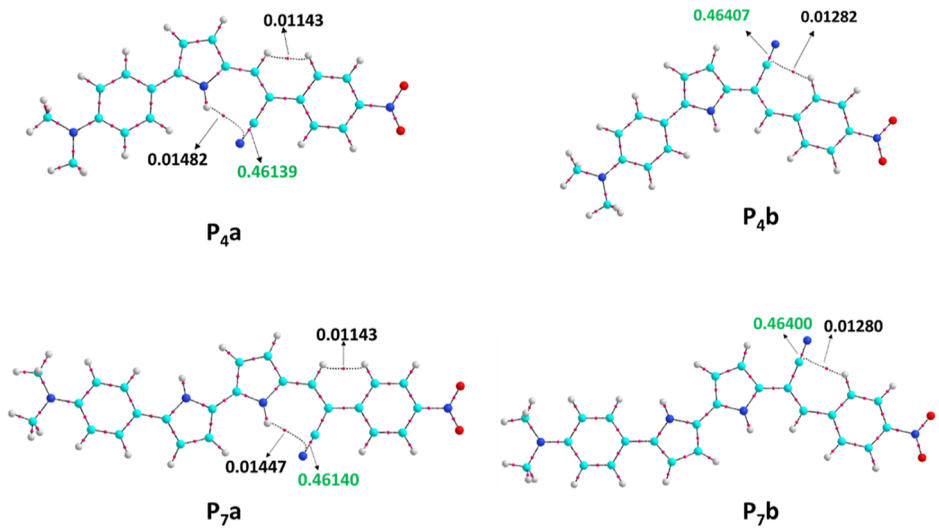

Figure 7. QTAIM features (ρ values in au) at the BCP of the relevant bond paths of both isomers of $\mathbf{P_4}$ and $\mathbf{P_7}$. Small red circles represent the BCPs.

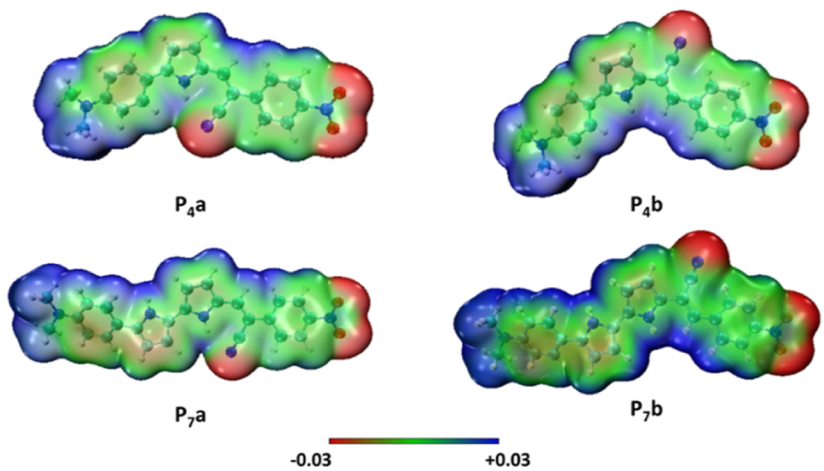

Figure 8. MESP distribution of $\mathbf{P_4}$ and $\mathbf{P_7}$ isomers represented on the 0.001 au electron density surface with color codes ranging from −0.03 au (red) to 0.03 au (blue).

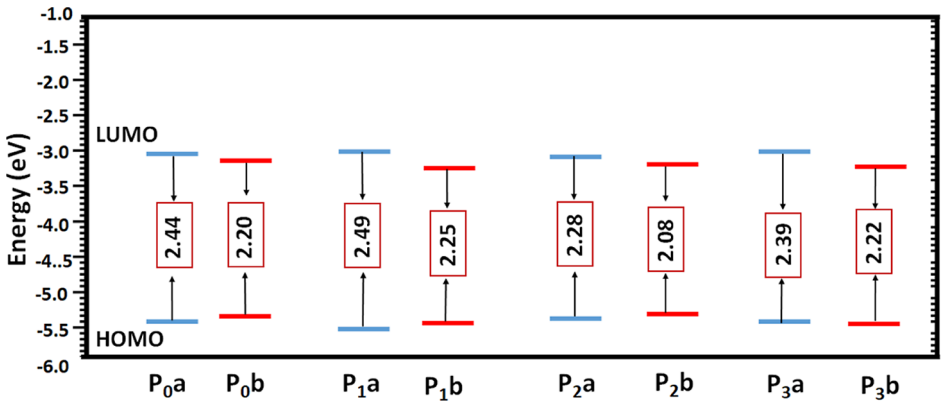

Figure 9. FMO energy level diagram of "**a**" and "**b**" variants of $\mathbf{P_0} - \mathbf{P_3}$.

is found to be the most stable molecule with ΔE_{HL} of 2.489 eV, which is higher than that of the reference molecule by 0.054 eV. Three molecules ($\mathbf{P_1a}$, $\mathbf{P_4a}$ & $\mathbf{P_5a}$) show more stability than the reference molecule, and all other molecules, irrespective of "**a**" or "**b**" isomers, tend to show higher reactivity with reduced ΔE_{HL} compared to that of the reference molecule. Molecules such as $\mathbf{P_6b}$, $\mathbf{P_7b}$, and $\mathbf{P_9b}$ show higher reactivity with lower ΔE_{HL} values of 1.960, 1.963, and 1.974 eV, respectively. Among "**a**" series, $\mathbf{P_6a}$, and $\mathbf{P_7a}$ are highly reactive with ΔE_{HL} values 2.151 and 2.188 eV, respectively. The reactivity increases when two heteroatoms are introduced into the molecular framework ($\mathbf{P_6} - \mathbf{P_9}$) which is observed

https://doi.org/10.1021/acsomega.4c00850
ACS Omega 2024, 9, 22764−22776

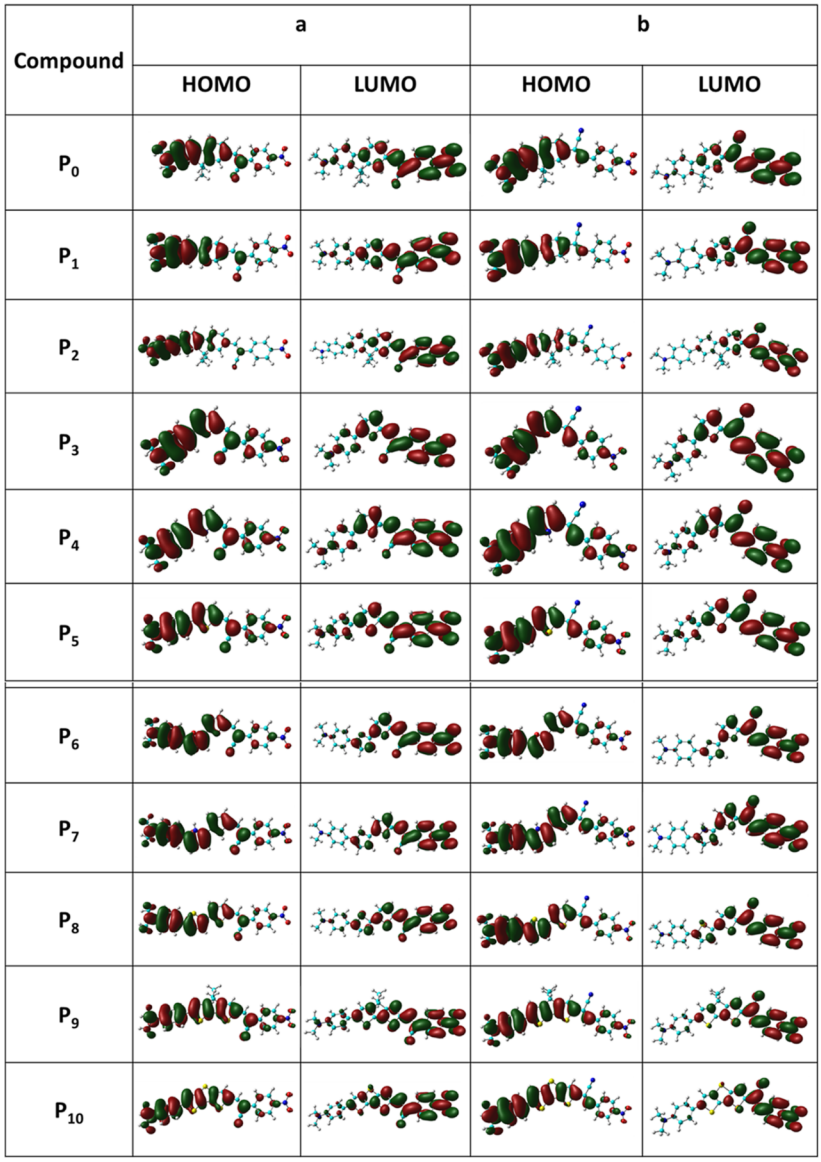

Figure 10. FMOs of the studied molecules.

from the computed ΔE_{HL}. On the other hand, the introduction of two heteroatoms does not alter the energy of HOMO a lot but does impact the LUMO energy level. It is observed that HOMO of **P$_6$a** and **P$_6$b** lies at −5.214 and −5.216 eV which clearly indicates that HOMO is almost unaffected by the position of the −CN group. However, the LUMO energy (−3.062 eV) of **P$_6$a** is altered to −3.257 eV when the position of the −CN group changes in the "**b**" isomer. The decreasing order of ΔE_{HL} in "**a**" isomer is as follows **P$_1$a** > **P$_5$a** > **P$_4$a** > **P$_0$a** > **P$_3$a** > **P$_2$a** > **P$_{10}$a** > **P$_8$a** > **P$_9$a** > **P$_7$a** > **P$_6$a** while the same for "**b**" isomer is **P$_5$b** > **P$_1$b** > **P$_4$b** > **P$_3$b** > **P$_0$b** > **P$_2$b** > **P$_{10}$b** > **P$_8$b** > **P$_9$b** > **P$_7$b** > **P$_6$b**. This clearly shows that irrespective of the position of the −CN group, **P$_6$**, **P$_7$**, and **P$_9$** are potential candidates with excellent chemical reactivity.

The FMOs such as HOMO and LUMO for both isomers are collected in Figure 10. From the figure, it is clear that the HOMO occupies the donor and a part of the π-bridge (left-hand side) while LUMO spread through the acceptor unit and the other part of the π-bridge (right-hand side). It is interesting to note that in "**a**" isomers, the −CN group involves in the stabilization of both HOMO & LUMO while its role in the stabilization of HOMO in the "**b**" isomers is zero. Thus, the HOMO of the "**a**" isomers is very similar to that of the "**b**" isomer except for the contribution of the −CN group. However, the LUMO of "**b**" isomers is observed to be very similar to that of "**a**" isomers where -the CN group is involved in stabilization. Analyzing the HOMOs and LUMOs of these molecules indicates that there can be intramolecular charge transfer (ICT) along with π−π* transitions. In some molecules, the π−π* transitions are expected to be predominant. For instance, the HOMO and LUMO of **P$_9$a** are lying on most of the molecule compared to **P$_2$a**. Thus, these molecules will tend to show both ICT and π−π* transitions in their absorption spectra.

To gain more insight into the FMOs, it is essential to understand how donor, acceptor, and π-bridge fragments contribute to the FMOs. The whole molecule is divided into three parts (donor, acceptor, and π-bridge), and their percentage contributions from these fragments toward HOMO and LUMO are calculated and summarized in Table S5 and Figure 11. In Figure 11, it is clear that the contribution of the donor unit to stabilizing LUMO is very negligible (0.1−

https://doi.org/10.1021/acsomega.4c00850
ACS Omega 2024, 9, 22764−22776

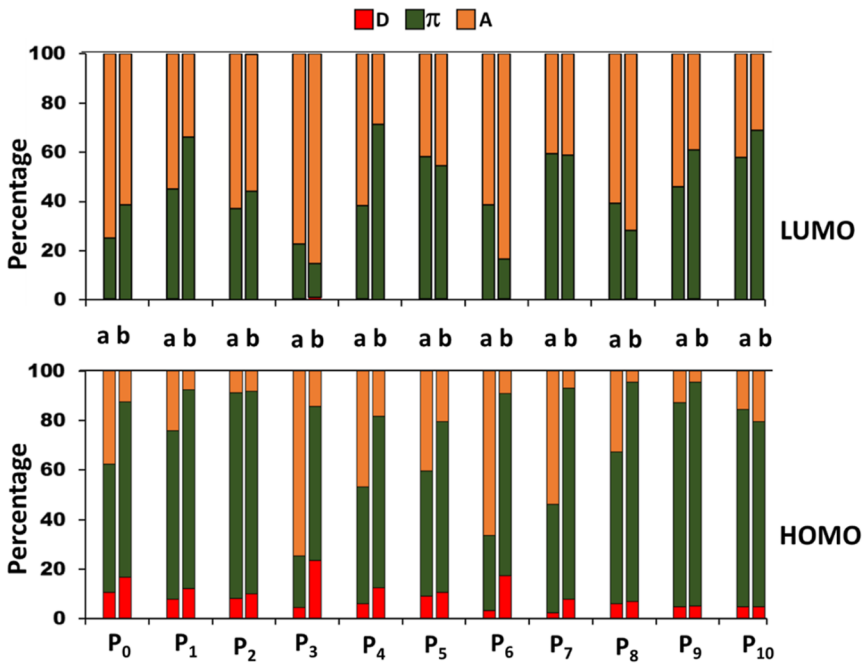

Figure 11. Percentage contributions of the fragments (donor, π-bridge, and acceptor) toward HOMO and LUMO of the studied molecules.

1%), while its contribution to HOMO varies from 2.5 to 23.4%. It is interesting to note that the donor's contribution to HOMO is higher in the "**b**" isomer compared to its "**a**" isomer except in $\mathbf{P_{10}b}$ where a slight edge (~0.1%) is observed. The results indicate that the LUMO gets many contributions from the acceptor unit, and a poor contribution is rendered by the acceptor unit toward the stabilization of HOMO. For instance, the LUMO of $\mathbf{P_6b}$ is stabilized up to 83.5% by the acceptor unit, while it gets only 9% toward HOMO. It is observed that the $\mathbf{P_3a}$, $\mathbf{P_5a}$, and $\mathbf{P_6a}$ molecules tend to get almost equal contributions from the acceptor unit for the stabilization of HOMO and LUMO. For example, the HOMO and LUMO of $\mathbf{P_5a}$ are stabilized by acceptor units almost equally (40.4 and 41.7%). Moving to the contribution of π-bridge, it can be inferred that HOMO is getting much contribution compared to LUMO. In particular, the HOMO of the "**b**" isomer largely benefited out of the π-bridge than the "**a**" isomer. In summary, this section portrays that the insertion of two heteroatoms tunes these molecules compared to those of one or none of the heteroatom-containing molecules.

3.6. Absorption Spectra. It is important to note that the molecule's ability to exhibit a significant absorption maximum makes it a promising candidate for optoelectronic applications.[73,74] In this context, TDDFT calculations on the optimized geometries help us in forecasting a molecule's excited state properties. Hence, TDDFT calculations have been conducted at the TD-BMK/SMD(dichloromethane)/6-31+G(d,p) level to compute the vertical singlet excitations to predict the absorption maxima with oscillatory strength. This analysis further helps us to estimate the percentage contributions from FMOs toward various configurations of these excitations. The details of the absorption spectra of "**a**" and "**b**" isomers, obtained through TDDFT calculations, for all the systems under study, are compared in Table 1. The optical properties studied include the absorption maxima (λ_{max}), oscillator strength (f), and the percentage contribution of different transitions toward the absorption maxima. In the "**a**" isomer series, the calculated λ_{max} ranges from 459 to 565 nm while the same applies to the "**b**" isomers ranging from 476 to 602 nm, and all transitions are from $S_0 \rightarrow S_1$. In both cases, the $\mathbf{P_2}$ molecule shows the lowest absorption maxima and $\mathbf{P_9}$ is the one that shows the highest absorption maxima. As expected, the $\mathbf{P_6b}$, $\mathbf{P_7b}$, and $\mathbf{P_9b}$ molecules show exceptional λ_{max} values of more than 590 nm. In all the cases, the consistent red shift in the λ_{max} value in the "**b**" isomer compared to the "**a**" isomer shows an increased wavelength of absorption as the position of the −CN group changes from the "**a**" to the "**b**" position. The shift in the λ_{max} value ranges from 17 nm (for the $\mathbf{P_2a} - \mathbf{P_2b}$ isomer pair) to 52 nm (for the $\mathbf{P_7a} - \mathbf{P_7b}$ isomer pair). This red shift in the absorption maximum can be attributed to the increase in planarity and the consequent increase in the effectiveness of π-delocalization. For instance, a 37 nm increase in λ_{max} is observed between the isomers "**a**" and "**b**" of $\mathbf{P_6}$ and $\mathbf{P_9}$. Another substantial increase in the λ_{max} is seen in $\mathbf{P_4}$ and $\mathbf{P_3}$ with 41 and 40 nm, respectively. It can be seen that the values of λ_{max} for all of the cases lie in the visible range, making them advisable for solar cell applications. The oscillator strengths (f), a measure of the intensity of absorption, show higher values for "**a**" isomers in all the cases. The difference in f values ranges from 0.320 (for the $\mathbf{P_3a} - \mathbf{P_3b}$ isomer pair) to 0.548 (for the $\mathbf{P_2a} - \mathbf{P_2b}$ isomer pair). For example, one can witness the strong intense peak at 459 with an oscillatory strength of 1.315 for $\mathbf{P_2a}$ and the same in $\mathbf{P_2b}$ that shows a less intense peak with an oscillatory strength of 0.767 for the 476 nm absorption. Hence, the intensity of absorption tends to be lower in the "**b**" isomer for all pairs of isomers under study though they tend to show longer λ_{max}. All these peaks are getting maximum contributions from HOMO → LUMO transitions for all these molecules, and minor contributions (less than 10%) are from HOMO−1 → LUMO. It is interesting to note that the HOMO → LUMO contributes to a higher percentage in the "**b**" isomer compared to that of the "**a**" isomer. For instance, an intense peak at 548 nm from $\mathbf{P_7a}$ arose due to an 87% contribution from HOMO → LUMO while its percentage increased to 93% for the peak at 600 nm when the position −CN changes in $\mathbf{P_7b}$. This trend is observed

https://doi.org/10.1021/acsomega.4c00850
ACS Omega 2024, 9, 22764−22776

Table 1. Maximum Absorption Wavelength (λ_{max}) along with Oscillator Strengths (f) and the MO Contribution of the Studied Molecules

isomer "a"				isomer "b"			
molecule	λ_{max} (nm)	f	MO contribution (in %)	molecule	λ_{max} (nm)	f	MO contribution (in %)
P_0a	486	1.334	H → L (87) H → L+1 (8) H−1 → L (4)	**P_0b**	515	0.834	H → L (93) H−1 → L (3) H → L+1 (3)
P_1a	461	1.186	H → L (86) H−1 → L (5) H → L+1 (8)	**P_1b**	481	0.728	H → L (92) H−1 → L (4) H → L+1 (3)
P_2a	459	1.315	H → L (78) H → L (12) H → L+1 (7)	**P_2b**	476	0.767	H → L (86) H−1 → L (10) H → L+1 (2)
P_3a	521	1.252	H → L (89) H−1 → L (3) H → L+1 (7)	**P_3b**	561	0.932	H → L (95) H−1 → L (2) H → L+1 (3)
P_4a	515	1.405	H → L (90) H−1 → L (3) H → L+1 (6)	**P_4b**	556	1.034	H → L (95) H−1 → L (3) H → L+1 (2)
P_5a	510	1.449	H → L (87) H−1 → L (4) H → L+1 (8)	**P_5b**	540	1.086	H → L (93) H−1 → L (3) H → L+1 (3)
P_6a	556	1.501	H → L (86) H−1 → L (5) H → L+1 (7)	**P_6b**	593	1.088	H → L (92) H−1 → L (5) H → L+1 (3)
P_7a	548	1.521	H → L (87) H−1 → L (6) H → L+1 (6)	**P_7b**	600	1.098	H → L (93) H−1 → L (4) H → L+1 (2)
P_8a	548	1.719	H → L (83) H−1 → L (7) H → L+1 (8)	**P_8b**	567	1.327	H → L (87) H−1 → L (7) H → L+1 (5)
P_9a	565	1.940	H → L (86) H−1 → L (5) H → L+1 (7)	**P_9b**	602	1.501	H → L (90) H−1 → L (5) H → L+1 (4)
P_{10}a	527	1.783	H → L (84) H−1 → L (7) H → L+1 (7)	**P_{10}b**	552	1.336	H → L (88) H−1 → L (7) H → L+1 (3)

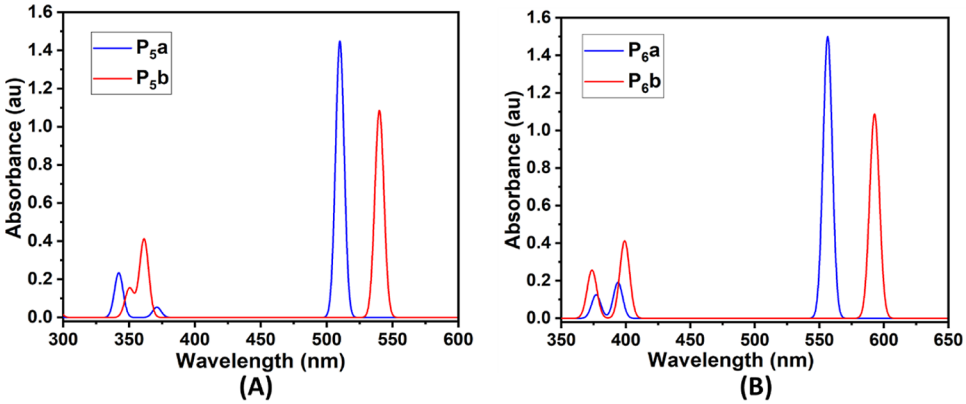

Figure 12. Comparison of simulated UV absorption spectra of (A) **P_5a** & **P_5b** (B) **P_6a** & **P_6b**.

for all of the molecules studied here. These HOMO → LUMO transitions can arise from ICT coupled with π−π^* transitions. For instance, **P_5a** tends to show a peak at 510 nm with 1.449 oscillator strength arising from HOMO → LUMO transition resulting from π−π^* transitions and ICT. This trend is observed in almost all the molecules. The UV absorption spectra of two pairs of "**a**" and "**b**" isomers *viz*. **P_5a** − **P_5b** pair and **P_6a** − **P_6b** pair in dichloromethane solvent are compared in Figure 12. The red shift in absorption maxima as well as the lowering of intensities in the "**b**" isomers can be clearly visualized in the figure.

3.7. NLO Properties. The NLO behavior of a molecule occurs due to the oscillation of molecular electrons when subjected to a fluctuating field, like electromagnetic radiation.[75−77] Consequently, this induces polarization within the molecule, and the effect becomes more prominent in D−π−A

https://doi.org/10.1021/acsomega.4c00850
ACS Omega 2024, 9, 22764−22776

molecules, generating asymmetric polarization. It is well known that electrons tend to migrate more readily toward the electron acceptor group rather than the donor group, contributing to this asymmetry.[78] As these molecules also fall under D−π−A architecture with excellent absorption maxima, it is intriguing to study their NLO properties.[79] We calculated the first-order hyperpolarizability (β_0) and second-order hyperpolarizability (γ) obtained at 1064 nm for all these molecules and the results are depicted in Figures 13 and 14, respectively. The data

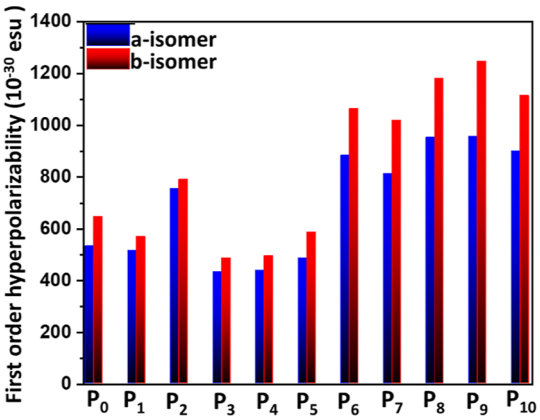

Figure 13. Comparison of β_0 values of the studied molecules.

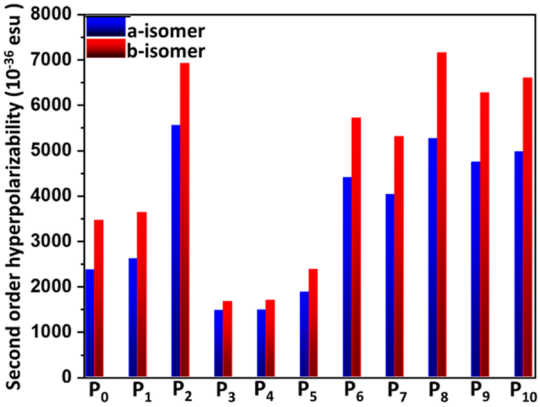

Figure 14. Comparison of γ values of the studied molecules.

pertaining to x, y, and z components of β_0 and γ are collected in Table S6. Our results show that the "**b**" isomers show better NLO activities compared to their "**a**" isomers. The computed first-order hyperpolarizabilities for $\mathbf{P_9a}$ are 955.62 × 10^{-30} esu, while the same for $\mathbf{P_9b}$ is estimated to be 1245.86 × 10^{-30} esu. A similar trend is observed for all of molecules. It is interesting to note that the molecules with lower ΔE_{HL} show higher β_0 values while those with wider ΔE_{HL} show lower β_0 values. For example, among all the molecules, $\mathbf{P_3a}$ shows the lowest β_0 value with 432.51 × 10^{-30} esu while $\mathbf{P_9b}$ shows the highest β_0 value of 1245.86 × 10^{-30} esu. Among the 22 scrutinized molecules, the "**b**" isomers of $\mathbf{P_6}$− $\mathbf{P_{10}}$ show higher β_0 values. Moving from the "**a**" isomer to the "**b**" isomer, there is an increase in the β_0 values and the increase is significantly pronounced in $\mathbf{P_9}$ where a shift of 290 × 10^{-30} esu, while this effect is minimum with only a small increment (35.45 × 10^{-30} esu), is observed in $\mathbf{P_2}$ isomers. The calculated results reveal that six of the ten designed candidates were found to show higher β_0 values and thus better NLO activity compared to the reference molecule $\mathbf{P_0}$. In general, the higher the chemical reactivity (lower the ΔE_{HL}), the higher the first-order hyperpolarizability.

Finally, we noted the γ values of the designed molecules, and the values are compared graphically in Figure 14. It can be inferred from Figure 14 that the isomers "**b**" show higher γ compared to the isomers "**a**". This is very similar to what we observed for first-order hyperpolarizability. The increment is very minimal in the case of $\mathbf{P_3}$, $\mathbf{P_4}$, and $\mathbf{P_5}$ while it is maximum in $\mathbf{P_8}$. Especially, $\mathbf{P_8b}$ has the maximum γ value followed by $\mathbf{P_2b}$ with 7147.22 × 10^{-36} esu and 6909.72 × 10^{-36} esu, respectively. Among the ten designed molecules, six of them showed higher γ values, suggesting the significance of modulating the π-bridge to tune the NLO properties of D−π−A type molecules.

4. CONCLUSIONS

In this study, we could attain significant theoretical insight into the effect of α and β cyano positional variation ("**a**" and "**b**" isomeric forms) on the structure, electronic, and optical properties of D−π−A-based cyanostilbene derivatives by means of DFT/TDDFT calculations. We designed ten different sets of D−π−A structures ($\mathbf{P_1}$ − $\mathbf{P_{10}}$) and their positional isomers from a reference compound $\mathbf{P_0a}$ by varying the π-linkers. The B3LYP/6-31+G(d,p) method was used to optimize the designed molecules, and the solvation effect was included wherever necessary with the dichloromethane solution using the SMD model. The findings reveal that the "**b**" isomers are less distorted from planarity compared to "**a**" and molecules having furanoid rings in their spacer groups are found to have better planarity. Comparisons of "**a**" and "**b**" isomers showed that the "**a**" isomer is more stable than "**b**" due to strong intramolecular interactions, as evident from the NCI and QTAIM analyses. The ΔE_{ba} values show the extent of stability of "**a**", and the highest (7.4 kcal/mol) and the lowest values (1.2 kcal/mol) are found for $\mathbf{P_4}$ and $\mathbf{P_1}$, respectively.

Further theoretical analyses reveal that the "**b**" isomers show higher chemical reactivity, higher absorption maxima, and higher hyperpolarizabilities compared to their "**a**" counterpart. Especially, the red shift in absorption maximum of "**b**" isomers arises from enhanced π-delocalization and planarity. Among all of them, $\mathbf{P_9b}$ tends to show the highest absorption maxima characterized by ICT coupled with π−π* transitions. NLO studies indicate that the molecules with reduced HOMO−LUMO gap show greater first and second-order hyperpolarizabilities. Overall, this study helps experimental scientists to design new molecules with D−π−A architecture with varying π-linkers, and the interplay between the chemical reactivity and other optoelectronic properties can be envisaged prior to synthesis.

■ ASSOCIATED CONTENT

Supporting Information

The Supporting Information is available free of charge at https://pubs.acs.org/doi/10.1021/acsomega.4c00850.

Optimized geometries of all studied structures, structural details, HOMO, LUMO energies, QTAIM results, and NLO values (PDF)

■ AUTHOR INFORMATION

Corresponding Authors

Pookkottu K. Sajith − *Department of Chemistry, Farook College (Autonomous), (Affiliated to the University of*

https://doi.org/10.1021/acsomega.4c00850
ACS Omega 2024, 9, 22764−22776

Calicut), Kozhikode 673632 Kerala, India; orcid.org/0000-0003-1574-8671; Email: pksajith@farookcollege.ac.in, pksajisiv@gmail.com

Rajadurai Vijay Solomon − *Department of Chemistry, Madras Christian College (Autonomous), (Affiliated to the University of Madras), Chennai 600059 Tamil Nadu, India*; Email: vjsolo@gmail.com, vjsolo@mcc.edu.in

Authors

Cherumannil Femina − *Department of Chemistry, Farook College (Autonomous), (Affiliated to the University of Calicut), Kozhikode 673632 Kerala, India;* orcid.org/0000-0001-5216-3643

Karunakaran Remya − *Government Women's Polytechnic College, Kozhikode 673009 Kerala, India*

Reji Thomas − *Department of Chemistry, Farook College (Autonomous), (Affiliated to the University of Calicut), Kozhikode 673632 Kerala, India*

Complete contact information is available at: https://pubs.acs.org/10.1021/acsomega.4c00850

Notes

The authors declare no competing financial interest.

■ ACKNOWLEDGMENTS

C.F. is thankful to DST-KIRAN for the Women Scientist-A fellowship (DST/WOS-A/CS-126/2021 (G) WISE KIRAN). P.K.S. and R.T. acknowledged Rashtriya Uchchatar Shiksha Abhiyan (RUSA) for the support. The authors thank M. Shanthil, Government Victoria College, Palakkad, Kerala, India for valuable suggestions.

■ REFERENCES

(1) Khasbaatar, A.; Xu, Z.; Lee, J.-H.; Campillo-Alvarado, G.; Hwang, C.; Onusaitis, B. N.; Diao, Y. From Solution to Thin Film: Molecular Assembly of π-Conjugated Systems and Impact on (Opto)Electronic Properties. *Chem. Rev.* **2023**, *123* (13), 8395−8487.

(2) Albano, G.; Pescitelli, G.; Di Bari, L. Chiroptical Properties in Thin Films of π-Conjugated Systems. *Chem. Rev.* **2020**, *120* (18), 10145−10243.

(3) Mahalingavelar, P.; Kanvah, S. α-Cyanostilbene: A Multifunctional Spectral Engineering Motif. *Phys. Chem. Chem. Phys.* **2022**, *24* (38), 23049−23075.

(4) Yoon, S.-J.; Varghese, S.; Park, S. K.; Wannemacher, R.; Gierschner, J.; Park, S. Y. Color-Tuned, Highly Emissive Dicyanodistyrylbenzene Single Crystals: Manipulating Intermolecular Stacking Interactions for Spontaneous and Stimulated Emission Characteristics. *Adv. Opt. Mater.* **2013**, *1* (3), 232−237.

(5) Femina, C.; Shanthil, M.; Sajith, P. K.; Thomas, R. Anthracene-Incorporated Cyanostilbene Based Donor-Acceptor Systems: Intramolecular Charge Transfer and Aggregation Induced Emission. *New J. Chem.* **2023**, *47* (29), 13810−13819.

(6) Martínez-Abadía, M.; Giménez, R.; Ros, M. B. Self-Assembled α-Cyanostilbenes for Advanced Functional Materials. *Adv. Mater.* **2018**, *30* (5), 1704161.

(7) König, N. F.; Mutruc, D.; Hecht, S. Accelerated Discovery of α-Cyanodiarylethene Photoswitches. *J. Am. Chem. Soc.* **2021**, *143* (24), 9162−9168.

(8) Jimenez, E. R.; Rodríguez, H. Aggregation-Induced Emission: A Review of Promising Cyano-Functionalized AIEgens. *J. Mater. Sci.* **2020**, *55* (4), 1366−1387.

(9) Martínez-Abadía, M.; Varghese, S.; Milián-Medina, B.; Gierschner, J.; Giménez, R.; Ros, M. B. Bent-Core Liquid Crystalline Cyanostilbenes: Fluorescence Switching and Thermochromism. *Phys. Chem. Chem. Phys.* **2015**, *17* (17), 11715−11724.

(10) Zhu, X.; Feng, L.; Cao, S.; Wang, J.; Niu, G. Donor-Acceptor-Acceptor-Conjugated Dual-State Emissive Acrylonitriles: Investigating the Effect of Acceptor Unit Order and Biological Imaging. *Org. Lett.* **2022**, *24* (45), 8305−8309.

(11) Ibrahim, N.; Loumaigne, M.; Grolleau, J.; Allain, M.; Frère, P. Dual-State Emission versus No Emission by Manipulating the Molecular Structures of Cyanovinyl-Benzofuran Derivatives. *Mol. Syst. Des. Eng.* **2022**, *7* (9), 1119−1128.

(12) Hang, C.; Wu, H.-W.; Zhu, L.-L. π-Conjugated Cyanostilbene-Based Optoelectric Functional Materials. *Chin. Chem. Lett.* **2016**, *27* (8), 1155−1165.

(13) Zhu, L.; Zhao, Y. Cyanostilbene-Based Intelligent Organic Optoelectronic Materials. *J. Mater. Chem. C* **2013**, *1* (6), 1059−1065.

(14) Anandhan, K.; Cerón, M.; Perumal, V.; Ceballos, P.; Gordillo-Guerra, P.; Pérez-Gutiérrez, E.; Castillo, A. E.; Thamotharan, S.; Percino, M. J. Solvatochromism and pH Effect on the Emission of a Triphenylimidazole-Phenylacrylonitrile Derivative: Experimental and DFT Studies. *RSC Adv.* **2019**, *9* (21), 12085−12096.

(15) Huang, Z.; Tang, F.; He, F.; Kong, L.; Huang, J.; Yang, J.; Ding, A. Pyrene and Triphenylamine Substituted Cyanostyrene and Cyanostilbene Derivatives with Dual-State Emission for High-Contrast Mechanofluorochromism and Cell Imaging. *Org. Chem. Front.* **2022**, *9* (19), 5118−5124.

(16) Fan, G.; Yan, D. Positional Isomers of Cyanostilbene: Two-Component Molecular Assembly and Multiple-Stimuli Responsive Luminescence. *Sci. Rep.* **2014**, *4* (1), 4933.

(17) Zhang, Y.; Zhuang, G.; Ouyang, M.; Hu, B.; Song, Q.; Sun, J.; Zhang, C.; Gu, C.; Xu, Y.; Ma, Y. Mechanochromic and Thermochromic Fluorescent Properties of Cyanostilbene Derivatives. *Dye. Pigment.* **2013**, *98* (3), 486−492.

(18) Yokoyama, S.; Nishiwaki, N. Fluorescence Behavior of Bis(Cyanostyryl)Pyrrole Derivatives Depending on the Substituent Position of Cyano Groups in Solution and in Solid State. *J. Org. Chem.* **2019**, *84* (3), 1192−1200.

(19) Zeng, C.; Dai, J.; Yang, T.; Wang, Z.; Gao, Y.; Xia, J.; Chen, Y.; Sun, M. Multi-Stimuli Fluorescence Responsiveness of α-Cyanostilbene Derivative: AIEE, Stimuli Response to Polarity, Acid, Force and Light, Applications in Anti-Counterfeiting and Single Phosphor w-OLED. *Dye. Pigment.* **2024**, *222*, 111906.

(20) Udayakumar, M.; Cerón, M.; Ceballos, P.; Percino, M. J.; Thamotharan, S. Interplay of Weak Noncovalent Interactions in Two Conjugated Positional Isomers: A Combined X-Ray, Optical Properties and Theoretical Investigation. *J. Mol. Struct.* **2019**, *1195*, 32−42.

(21) Castillo, A.; Ceballos, P.; Santos, P.; Cerón, M.; Venkatesan, P.; Pérez-Gutiérrez, E.; Sosa-Rivadeneyra, M.; Thamotharan, S.; Siegler, M. A.; Percino, M. J. Solution and Solid-State Photophysical Properties of Positional Isomeric Acrylonitrile Derivatives with Core Pyridine and Phenyl Moieties: Experimental and DFT Studies. *Molecules* **2021**, *26* (6), 1500.

(22) Zeng, S.; Yin, L.; Ji, C.; Jiang, X.; Li, K.; Li, Y.; Wang, Y. D-π-A-π-D Type Benzothiadiazole-Triphenylamine Based Small Molecules Containing Cyano on the π-Bridge for Solution-Processed Organic Solar Cells with High Open-Circuit Voltage. *Chem. Commun.* **2012**, *48* (86), 10627−10629.

(23) Wang, X.; Ding, Z.; Ma, Y.; Zhang, Y.; Shang, H.; Jiang, S. Multi-Stimuli Responsive Supramolecular Gels Based on a D-π-A Structural Cyanostilbene Derivative with Aggregation Induced Emission Properties. *Soft Matter* **2019**, *15* (7), 1658−1665.

(24) El-Meligy, A. B.; Koga, N.; Iuchi, S.; Yoshida, K.; Hirao, K.; Mangood, A. H.; El-Nahas, A. M. DFT/TD-DFT Calculations of the Electronic and Optical Properties of Bis-N,N-Dimethylaniline-Based Dyes for Use in Dye-Sensitized Solar Cells. *J. Photochem. Photobiol. A Chem.* **2018**, *367*, 332−346.

(25) Majumder, R.; Dey, S.; Jana, D.; Ghorai, B. K. Donor-Acceptor Cyanostilbene Based Nano-AIEgens: Synthesis and Properties. *Results Chem.* **2023**, *5*, 100856.

(26) Lim, H. C.; Kim, J.-J.; Jang, J.; Hong, J.-I. Effect of the π-Linker on the Performance of Organic Photovoltaic Devices Based on Push-Pull D-π-A Molecules. *New J. Chem.* **2018**, *42* (14), 11458−11464.
(27) Sajid, H.; Ayub, K.; Gilani, M. A.; Mahmood, T. Donor-π-Acceptor N-Methyl-4,5-Diazacarbazole Based Ultra-High Performance Organic Solar Cells: A Density Functional Theory Study. *Energy Technol.* **2023**, *11* (1), 2201164.
(28) Bedoura, S.; Xi, H.-W.; Goh, H. W.; Lim, K. H. DFT/TDDFT Investigation on Donor-Acceptor Triazole-Based Copolymers for Organic Photovoltaics. *J. Mol. Struct.* **2022**, *1248*, 131406.
(29) Zaier, R.; Martel, A.; Antosiewicz, T. J. Effect of Benzothiadiazole-Based π-Spacers on Fine-Tuning of Optoelectronic Properties of Oligothiophene-Core Donor Materials for Efficient Organic Solar Cells: A DFT Study. *J. Phys. Chem. A* **2023**, *127* (50), 10555−10569.
(30) Shivani; Mishra, A.; Kaur, P.; Singh, K. Synthesis and Nonlinear Optical Behavior of Thermally Stable Chromophores Based on 9,9-Dimethyl-9H-Fluoren-2-Amine: Improving Intrinsic Hyperpolarizability through Modulation of "Push-Pull. *ACS Omega* **2022**, *7* (43), 39045−39060.
(31) Shivani; Mishra, A.; Kaur, P.; Singh, K. Perpetual Extension of Conjugation of Fluorene-Based Donor-Acceptor Dyads Yield Diminished Nonlinear Optical Response. *J. Phys. Chem. C* **2023**, *127* (2), 1260−1272.
(32) Gong, L.; Ma, C.; Liu, T.; Lv, J.; Xun, X. Theoretical Study on Functionalized Acrylonitrile Compounds with a Large Second-Order Nonlinear Optical Response. *New J. Chem.* **2020**, *44* (45), 19623−19629.
(33) Shivani; Mishra, A.; Kumar, V.; Kaur, P.; Singh, K. Synthesis, Linear and Non-Linear Optical Properties of "Push-Pull" Chromophores Based on 9,9-Dimethyl-9H-Fluoren-2-Amine. *Dye. Pigment.* **2022**, *200*, 110160.
(34) Kaur, P.; Singh, K. Second-Order Nonlinear Polarizability of "Push-Pull" Chromophores. A Decade of Progress in Donor-π-Acceptor Materials. *Chem. Rec.* **2022**, *22* (6), No. e202200024.
(35) Shivani; Kaur, I.; Chemmanghattu, K.; Kaur, P.; Singh, K. Non-Linear Optical Behavior of Benzothiazole Based Chromophores: Second Harmonic Generation. *Dye. Pigment.* **2020**, *183*, 108739.
(36) Khan, M. A.; Ayub, A. R.; Alrowaili, Z. A.; Ilyas, M.; Hui, L.; Abbas, S. Z. Self-Assembly of 2D Coordination Complex of Cytidine Monophosphate to Boost up the Optical Phenomena. *J. Mol. Struct.* **2022**, *1268*, 133655.
(37) Akram, S. J.; Hadia, N. M. A.; Iqbal, J.; Mehmood, R. F.; Iqbal, S.; Shawky, A. M.; Asif, A.; Somaily, H. H.; Raheel, M.; Khera, R. A. Impact of Various Heterocyclic π-Linkers and Their Substitution Position on the Opto-Electronic Attributes of the A-π-D-π-A Type IECIO-4F Molecule: A Comparative Analysis. *RSC Adv.* **2022**, *12* (32), 20792−20806.
(38) Sun, Z.-Z.; Long, R. Thia[5]Helicene-Based D-π-A-Type Molecular Semiconductors for Stable and Efficient Perovskite Solar Cells: A Theoretical Study. *J. Phys. Chem. C* **2023**, *127* (19), 8953−8962.
(39) Rehman, F. U.; Hameed, S.; Khera, R. A.; Shaban, M.; Essid, M.; Aloui, Z.; Al-Saeedi, S. I.; Ibrahim, M. A. A.; Waqas, M. High-Efficiency and Low-Energy-Loss Organic Solar Cells Enabled by Tuning the End Group Modification of the Terthiophene-Based Acceptor Molecules to Enhance Photovoltaic Properties. *ACS Omega* **2023**, *8* (45), 42492−42510.
(40) Zaier, R.; Ayachi, S. *Designing Well-Organized Donor-Bridge-Acceptor Conjugated Systems Based on Cyclopentadithiophene as Donors in Bulk Heterojunction Organic Solar Cells: DFT-Based Modeling and Calculations*; Elseman, A. M., Ed.; IntechOpen: Rijeka, 2021; Chapter 5.
(41) Bader, R. F. W. A Quantum Theory of Molecular Structure and Its Applications. *Chem. Rev.* **1991**, *91* (5), 893−928.
(42) Bader, R. F. W. Atoms in Molecules. *Acc. Chem. Res.* **1985**, *18* (1), 9−15.
(43) Johnson, E. R.; Keinan, S.; Mori-Sánchez, P.; Contreras-García, J.; Cohen, A. J.; Yang, W. Revealing Noncovalent Interactions. *J. Am. Chem. Soc.* **2010**, *132* (18), 6498−6506.
(44) Politzer, P.; Landry, S. J.; Waernheim, T. Proposed Procedure for Using Electrostatic Potentials to Predict and Interpret Nucleophilic Processes. *J. Phys. Chem.* **1982**, *86* (24), 4767−4771.
(45) Frisch, M. J.; Trucks, G. W.; Schlegel, H. B.; Scuseria, G. E.; Robb, M. A.; Cheeseman, J. R.; Scalmani, G.; Barone, V.; Petersson, G. A.; Nakatsuji, H.; et al. *Gaussian 16*. Revision B.01; Gaussian, Inc.: Wallingford, CT, 2016.
(46) Becke, A. D. Density-functional Thermochemistry. III. The Role of Exact Exchange. *J. Chem. Phys.* **1993**, *98* (7), 5648−5652.
(47) Lee, C.; Yang, W.; Parr, R. G. Development of the Colle-Salvetti Correlation-Energy Formula into a Functional of the Electron Density. *Phys. Rev. B* **1988**, *37* (2), 785−789.
(48) Zhurko, G. *Chemcraft 1.8 Program*: Ivanovo, Russia, 2005. https://chemcraftprog.com.
(49) Tenderholt; Adam, L. *"QMForge: A Program to Analyze Quantum Chemistry Calculations"*. Version 3.2. https://qmforge.net.
(50) Lu, T.; Chen, F. Multiwfn: A Multifunctional Wavefunction Analyzer. *J. Comput. Chem.* **2012**, *33* (5), 580−592.
(51) Keith, T. A. *AIMAll Program*. version 17.11.14; TK Gristmill Software: Overland Park KS, USA, 2017. http://aim.tkgristmill.com.
(52) Humphrey, W.; Dalke, A.; Schulten, K. VMD: Visual Molecular Dynamics. *J. Mol. Graph.* **1996**, *14* (1), 33−38.
(53) Yanai, T.; Tew, D. P.; Handy, N. C. A New Hybrid Exchange-Correlation Functional Using the Coulomb-Attenuating Method (CAM-B3LYP). *Chem. Phys. Lett.* **2004**, *393* (1−3), 51−57.
(54) Adamo, C.; Barone, V. Toward Reliable Density Functional Methods without Adjustable Parameters: The PBE0Model. *J. Chem. Phys.* **1999**, *110* (13), 6158−6170.
(55) Boese, A. D.; Martin, J. M. L. Development of Density Functionals for Thermochemical Kinetics. *J. Chem. Phys.* **2004**, *121* (8), 3405−3416.
(56) Marenich, A. V.; Cramer, C. J.; Truhlar, D. G. Universal Solvation Model Based on Solute Electron Density and on a Continuum Model of the Solvent Defined by the Bulk Dielectric Constant and Atomic Surface Tensions. *J. Phys. Chem. B* **2009**, *113* (18), 6378−6396.
(57) Liang, J.; Feng, X.; Hait, D.; Head-Gordon, M. Revisiting the Performance of Time-Dependent Density Functional Theory for Electronic Excitations: Assessment of 43 Popular and Recently Developed Functionals from Rungs One to Four. *J. Chem. Theory Comput.* **2022**, *18* (6), 3460−3473.
(58) Zhang, T.; Zhu, G.; Lin, L.; Mu, J.; Ai, B.; Li, Y.; Zhuo, S. Cyano Substitution Effect on the Emission Quantum Efficiency in Stilbene Derivatives: A Computational Study. *Org. Electron.* **2019**, *68*, 264−270.
(59) O'boyle, N. M.; Tenderholt, A. L.; Langner, K. M. Cclib: A Library for Package-Independent Computational Chemistry Algorithms. *J. Comput. Chem.* **2008**, *29* (5), 839−845.
(60) Kurtz, H. A.; Stewart, J. J. P.; Dieter, K. M. Calculation of the Nonlinear Optical Properties of Molecules. *J. Comput. Chem.* **1990**, *11* (1), 82−87.
(61) Bella, A. P.; Solomon, R. V.; Vedha, S. A.; Merlin, J. P. Enhanced Luminescence Efficiency of Structurally Tailored New Coumarin-Based Heterocyclic Organic Materials: A DFT/TD-DFT Study. *Theor. Chem. Acc.* **2019**, *138* (4), 53.
(62) Panneerselvam, M.; Kathiravan, A.; Solomon, R. V.; Jaccob, M. The Role of π-Linkers in Tuning the Optoelectronic Properties of Triphenylamine Derivatives for Solar Cell Applications - A DFT/TDDFT Study. *Phys. Chem. Chem. Phys.* **2017**, *19* (8), 6153−6163.
(63) Zhao, C.; Lu, Y.; Zhu, Z.; Liu, H. Theoretical Exploration of Halogen Bonding Interactions in the Complexes of Novel Nitroxide Radical Probes and Comparison with Hydrogen Bonds. *J. Phys. Chem. A* **2018**, *122* (22), 5058−5068.
(64) Ganie, A. A.; Rashid, S.; Ahangar, A. A.; Ismail, T. M.; Sajith, P. K.; Dar, A. A. Expanding the Scope of Hydroxyl-Pyridine Supra-

molecular Synthon to Design Molecular Solids. *Cryst. Growth Des.* **2022**, *22* (3), 1972−1983.
(65) Abdulla, H. M.; Gangwar, P.; Sajith, P. K.; Ramachandran, C. N. Probing the Interaction of NO with C_{60}: Comparison between Endohedral and Exohedral Complexes. *J. Phys. Chem. A* **2023**, *127* (16), 3598−3607.
(66) Sajith, P. K.; Suresh, C. H. Mechanisms of Reductive Eliminations in Square Planar Pd(II) Complexes: Nature of Eliminated Bonds and Role of Trans Influence. *Inorg. Chem.* **2011**, *50* (17), 8085−8093.
(67) Ganie, A. A.; Ismail, T. M.; Sajith, P. K.; Dar, A. A. Validation of the Supramolecular Synthon Preference through DFT and Physicochemical Property Investigations of Pyridyl Salts of Organo-Sulfonates. *New J. Chem.* **2021**, *45* (10), 4780−4790.
(68) Murray, J. S.; Politzer, P. The Electrostatic Potential: An Overview. *Wiley Interdiscip. Rev.: Comput. Mol. Sci.* **2011**, *1* (2), 153−163.
(69) Ismail, T. M.; Mohan, N.; Sajith, P. K. Theoretical Study of Hydrogen Bonding Interactions in Substituted Nitroxide Radicals. *New J. Chem.* **2021**, *45* (8), 3866−3875.
(70) Sajith, P. K.; Suresh, C. H. Quantification of the Trans Influence in Hypervalent Iodine Complexes. *Inorg. Chem.* **2012**, *51* (2), 967−977.
(71) Woodward, R. B.; Hoffmann, R. The Conservation of Orbital Symmetry. *Angew. Chem., Int. Ed. Engl.* **1969**, *8* (11), 781−853.
(72) El-Demerdash, S. H.; Halim, S. A.; El-Nahas, A. M.; El-Meligy, A. B. A Density Functional Theory Study of the Molecular Structure, Reactivity, and Spectroscopic Properties of 2-(2-Mercaptophenyl)-1-Azaazulene Tautomers and Rotamers. *Sci. Rep.* **2023**, *13* (1), 15626.
(73) Samuvel Michael, D.; Serangolam Krishnasami, S.; Vijay Solomon, R. A Two-Step MM and QM/MM Approach to Model AIEE of Aryloxy Benzothiadiazole Derivatives for Optoelectronic Applications. *Phys. Chem. Chem. Phys.* **2022**, *24* (6), 4051−4064.
(74) Francis, R. R.; Ebenezer, C.; Vijay Solomon, R.; Wilson, P. Computational Assessment of Amino Acid-Coupled Benzanthrone 2-Aminoacetamides as Molecular Probes for Insulin Amyloid Fibril Visualization. *New J. Chem.* **2023**, *47* (28), 13247−13259.
(75) Noudem, P.; Fouejio, D.; Mveme, C. D. D.; Nya, F. T.; Zekeng, S. S. Electronic, Nonlinear Optical, UV-Vis and NBO Analysis of Methyl Methacrylate for Optoelectronic and Optical Applications: DFT Study and Impact of Conformation. *Spectrochim. Acta Part A Mol. Biomol. Spectrosc.* **2023**, *303*, 123267.
(76) Hannachi, D.; Khelfaoui, N.; Zaidi, M.; Yahiaoui, D.; Lakehal, S.; Morell, C.; Chermette, H. The Effect of Resonance-Assisted Hydrogen Bond on the Second-Order Nonlinear Optical Properties of Pyridine Hydrazone Photoswitches: A Quantum Chemistry Investigation. *New J. Chem.* **2023**, *47* (39), 18359−18373.
(77) Kamli, D.; Hannachi, D.; Samsar, D.; Chermette, H. Bis-TTF-Ge Derivatives: Promising Linear and Nonlinear Optical Properties, a Theoretical Investigation. *New J. Chem.* **2023**, *47* (3), 1234−1246.
(78) Khalid, M.; Zafar, M.; Hussain, S.; Asghar, M. A.; Khera, R. A.; Imran, M.; Abookleesh, F. L.; Akram, M. Y.; Ullah, A. Influence of End-Capped Modifications in the Nonlinear Optical Amplitude of Nonfullerene-Based Chromophores with a D-π-A Architecture: A DFT/TDDFT Study. *ACS Omega* **2022**, *7* (27), 23532−23548.
(79) Khalid, M.; Naz, S.; Mahmood, K.; Hussain, S.; Carmo Braga, A. A.; Hussain, R.; Ragab, A. H.; Al-Mhyawi, S. R. First Theoretical Probe for Efficient Enhancement of Optical Nonlinearity via Structural Modifications into Phenylene Based D-π-A Configured Molecules. *RSC Adv.* **2022**, *12* (48), 31192−31204.

https://doi.org/10.1021/acsomega.4c00850
ACS Omega 2024, 9, 22764−22776